# A tau homeostasis signature is linked with the cellular and regional vulnerability of excitatory neurons to tau pathology

Hongjun Fu [1,2,3]*, Andrea Possenti[4], Rosie Freer[4], Yoshikazu Nakano[1], Nancy C. Hernandez Villegas[1], Maoping Tang[5], Paula V. M. Cauhy[1,8], Benjamin A. Lassus[1], Shuo Chen[1], Stephanie L. Fowler[1], Helen Y. Figueroa[1], Edward D. Huey[1,6], Gail V. W. Johnson[5], Michele Vendruscolo [4]* and Karen E. Duff [1,2,7]*

**Excitatory neurons are preferentially impaired in early Alzheimer's disease but the pathways contributing to their relative vulnerability remain largely unknown. Here we report that pathological tau accumulation takes place predominantly in excitatory neurons compared to inhibitory neurons, not only in the entorhinal cortex, a brain region affected in early Alzheimer's disease, but also in areas affected later by the disease. By analyzing RNA transcripts from single-nucleus RNA datasets, we identified a specific tau homeostasis signature of genes differentially expressed in excitatory compared to inhibitory neurons. One of the genes, BCL2-associated athanogene 3 (BAG3), a facilitator of autophagy, was identified as a hub, or master regulator, gene. We verified that reducing BAG3 levels in primary neurons exacerbated pathological tau accumulation, whereas BAG3 overexpression attenuated it. These results define a tau homeostasis signature that underlies the cellular and regional vulnerability of excitatory neurons to tau pathology.**

Neurodegenerative disorders are characterized by the accumulation of pathological proteins and the progressive loss of specific neuronal cell populations. The accumulation of misfolded tau aggregates is a defining feature of Alzheimer's disease (AD) and frontotemporal lobar degeneration (FTLD) linked to tau[1–3]. Several types of neurons have been reported to be particularly vulnerable in AD[4–9], Down's syndrome[10], and FTLD[2,3,11]. The distribution of neurons vulnerable to tauopathy follows a sequential pattern that suggests that cell populations in different regions of the brain are selectively at risk. More specifically, the morphology and location of cells within the entorhinal cortex (EC) and hippocampus that accumulate tau and degenerate in the earliest stages of AD suggest that excitatory (EX) neurons are preferentially impacted[4,12]. Previous studies have addressed the question of why putative EX neurons could be particularly vulnerable to degeneration in aging, AD, and other neurodegenerative disorders[6,13–15]. Determinants of neuronal vulnerability might include cell size and location within neural circuits, signaling pathways controlling excitation, mechanisms regulating calcium and energy homeostasis, metabolism of disease-specific proteins, repertoires of signal-transduction pathways and stress-resistance mechanisms, and protein homeostasis dysfunction[16–19]. However, the exact molecular determinants underlying the selective vulnerability of EX neurons to tau pathology have not been established.
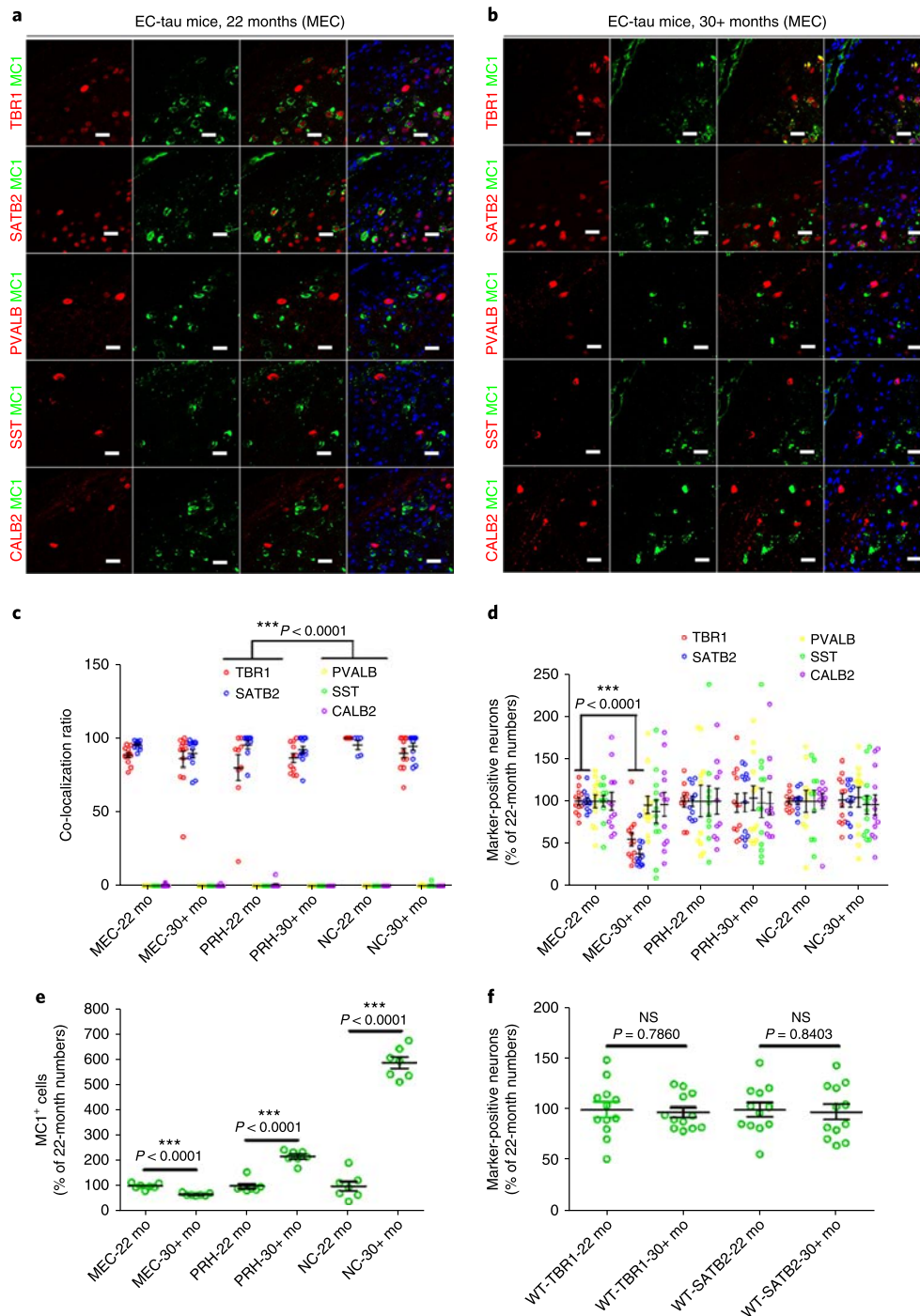
To explore these determinants, we employed four complementary approaches. First, using a series of cell-type-specific markers on AD patient brains and a mouse model of tauopathy[20], we showed that tau co-localizes predominantly with EX, compared to inhibitory (IN), neuron markers, not only in the EC but also in areas affected later in the disease such as the neocortex[4]. Second, using single-nucleus RNA-seq datasets from normal donors, we identified a substantial difference between EX and IN neurons in genes involved in a branch of the protein homeostasis system that modulates the aggregation and clearance of tau. Third, using the weighted gene co-expression network analysis, we identified that BAG3, a putative aggregation protector[21,22], is a hub gene in the co-expression network relevant to tau homeostasis. Lastly, we confirmed that BAG3 is differentially expressed in human EX and IN neurons in non-AD and AD brains and that it impacts tau accumulation in primary neurons. Taken together, these results support the conclusion that tau homeostasis contributes to the selective regional vulnerability of EX neurons to tau pathology and cell loss that defines AD, and they suggest that dysregulation of specific branches of the protein homeostasis system plays an important role in the initiation and spread of tau pathology in AD and the primary tauopathies.

## Results

**Excitatory and inhibitory neurons are differentially vulnerable to tau pathology in primary and secondary affected regions of EC-tau mice.** Tau species recognized by human-specific antibodies such as MC1 (which targets misfolded tau) were co-localized with EX neuronal markers (TBR1 and SATB2), but there was almost no co-localization with IN neuronal markers (PVALB, SST, and CALB2) in layers II–IV of the medial entorhinal cortex (MEC), perirhinal cortex (PRH), and neocortex (NC) of EC-tau mice[20] at
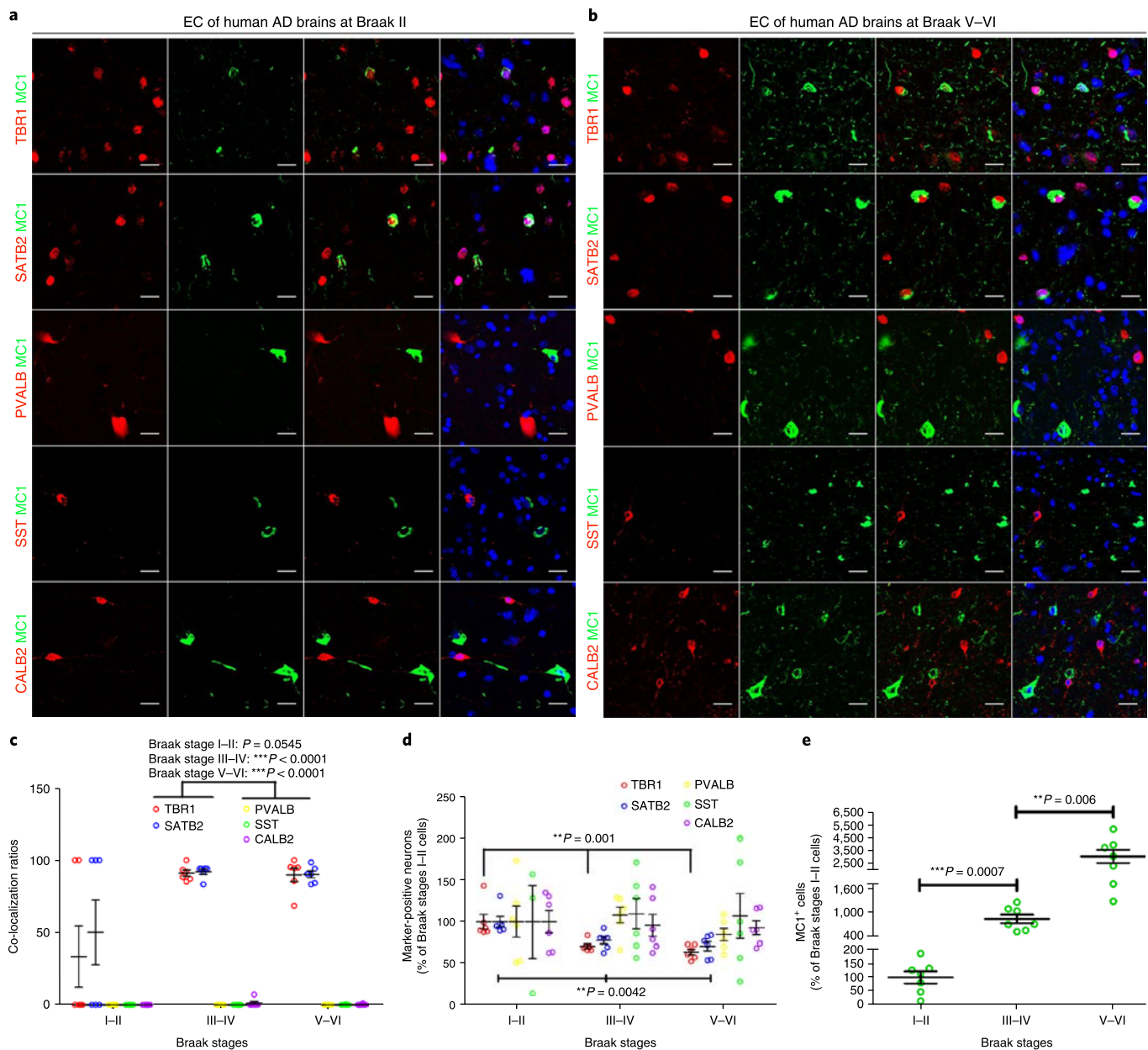
**Fig. 1 | Excitatory and inhibitory neurons are differentially vulnerable to tau pathology in primary and secondary affected regions of EC-tau mice.**
**a,b**, Representative images of MC1^{+} tau staining co-localized with TBR1^{+} and SATB2^{+} EX neurons, but not PVALB[+], SST[+], or CALB2^{+} IN neurons, in the MEC of EC-tau mice at 22 months (**a**) and at 30+ months (**b**). Three independent experiments were repeated with similar results. Scale bar, 20 μm.
**c**, Co-localization ratios of MC1^{+} tau with neuronal marker-positive neurons, quantified in the MEC, PRH, and NC (layers II–IV) of EC-tau mice at 22 and 30+ months (***$P < 0.0001$ vs. PVALB, SST, and CALB2 in mice matched for brain region and age; Kruskal–Wallis statistics: 53.16 for MEC of 22-month-old mice (MEC-22 mo), 53.09 for MEC of 30+-month-old mice (MEC-30+ mo), 41.17 for PRH of 22-month-old mice (PRH-22 mo), 49.65 for PRH of 30+-month-old mice (PRH-30+ mo), 29.37 for NC of 22-month-old mice (NC-22 mo), and 48.02 for NC of 30+-month-old mice (NC-30+mo)).
**d,e**, Numbers of (**d**) neuronal marker-positive neurons (***$P < 0.0001$ 22 months vs. 30+ months in matched brain regions and neuronal markers; $R^2 = 0.6996$, $F = 34.16$) and (**e**) MC1^{+} cells, counted in the above regions of EC-tau mice at 22 and 30+ months (***$P < 0.0001$ 30+ months vs. 22 months; $t_{12} = 6.921$ for MEC, $t_{12} = 8.833$ for PRH, $t_{12} = 16.56$ for NC). **f**, Numbers of TBR1^{+} and SATB2^{+} EX neurons compared in the MEC of non-transgenic (wild-type, WT) mice at 22 and 30+ months (NS, not significant, 30+ months vs. 22 months; $t_{22} = 0.2748$ for TBR1^{+} and $t_{22} = 0.2040$ for SATB2^{+}). Data are presented as mean ± s.e.m. In **c**, **d**, **f**, $n = 6$ animals, 2 sections per animal; sections with no MC1^{+} neurons were removed from further analysis, for example, PRH 22 months: $n = 9$; PRH 30+ months: $n = 11$; NC 22 months: $n = 6$; NC 30+ months: $n = 11$ independent sections); in **e**, $n = 7$ independent experiments and each value is the average of 12 biological independent sections. Statistical significance was assessed by Kruskal–Wallis test with Dunn's multiple-comparison test (**c**) and one-way ANOVA with Tukey's post test (**d**). In **e**, **f**, statistical significance was assessed by two-tailed unpaired $t$ test.

**Fig. 2 | EX and IN human neurons are differentially vulnerable to tau pathology in primary affected regions of AD brain. a,b,** Representative images of MC1^{+} tau staining co-localized with TBR1^{+} and SATB2^{+} EX neurons, but not PVALB[+], SST[+], or CALB2^{+} IN neurons, in the EC of AD patient brain at Braak stages (**a**) II and (**b**) V–VI. Three independent experiments were repeated with similar results. Scale bar, 20 μm. **c,** Co-localization ratio of MC1^{+} tau with neuronal marker-positive neurons, quantified in EC layers II–IV of AD brains at different Braak stages; data are presented as mean ± s.e.m. ($n=3$ brains, 2 sections per brain, Kruskal–Wallis test with Dunn's multiple-comparison test, ***$P < 0.0001$ vs. PVALB, SST, and CALB2 at matched Braak stages; Kruskal–Wallis statistics: 9.280, 25.82, and 24.90, respectively.). **d,e,** Numbers of (**d**) neuronal marker-positive neurons and (**e**) MC1^{+} cells, assessed in EC layers II–IV of AD brains at different Braak stages; data are shown as the percentage of the average number of neuronal marker-positive cells at Braak stages I–II and are presented as mean ± s.e.m. ($n=3$ brains, 2 sections per brain, (**d**) one-way ANOVA with Tukey's multiple comparison post hoc tests; $R^2 = 0.6026$, $F = 11.37$ for TBR1^{+} neurons; $R^2 = 0.5187$, $F = 8.082$ for SATB2^{+} neurons; (**e**) two-tailed unpaired $t$ test with Welch's correction; **$P < 0.01$; ***$P < 0.001$ vs. Braak stages I–II; $t_6 = 6.369$ for Braak stage III-IV, $t_6 = 4.150$ for Braak stage V–VI).

either 22 or 30+ months of age (Fig. 1a–c and Supplementary Fig. 1). These results are consistent with the observation of limited co-localization of human tau with IN neurons in the dentate gyrus of this mouse model[23]. In addition to being differentially vulnerable to pathological tau accumulation, EX neurons in the MEC were also differentially vulnerable to cell loss. The number of EX neurons was significantly reduced in the MEC, but not in the PRH or NC regions of EC-tau mice at 30+ months compared with 22 months

(Fig. 1d). However, there was no significant difference in the number of IN neurons in EC-tau mice at 30+ months compared with 22 months (Fig. 1d). The number of MC1^{+} neurons was also significantly reduced in the MEC of EC-tau mice at 30+ months compared with 22 months (Fig. 1e), most likely due to the dramatic loss of EX neurons in that region (Fig. 1d). There was no significant difference in the number of EX neurons in nontransgenic (wild-type) mice between 22 months and 30+ months (Fig. 1f), indicating that the
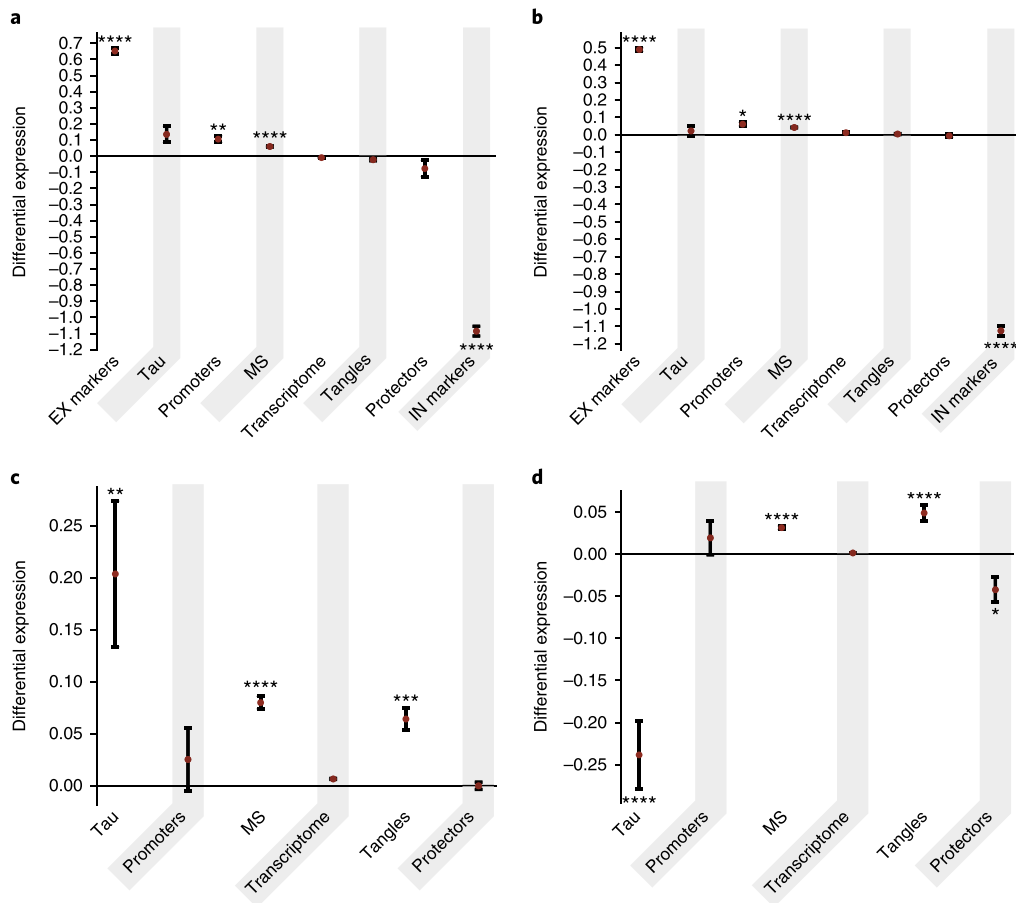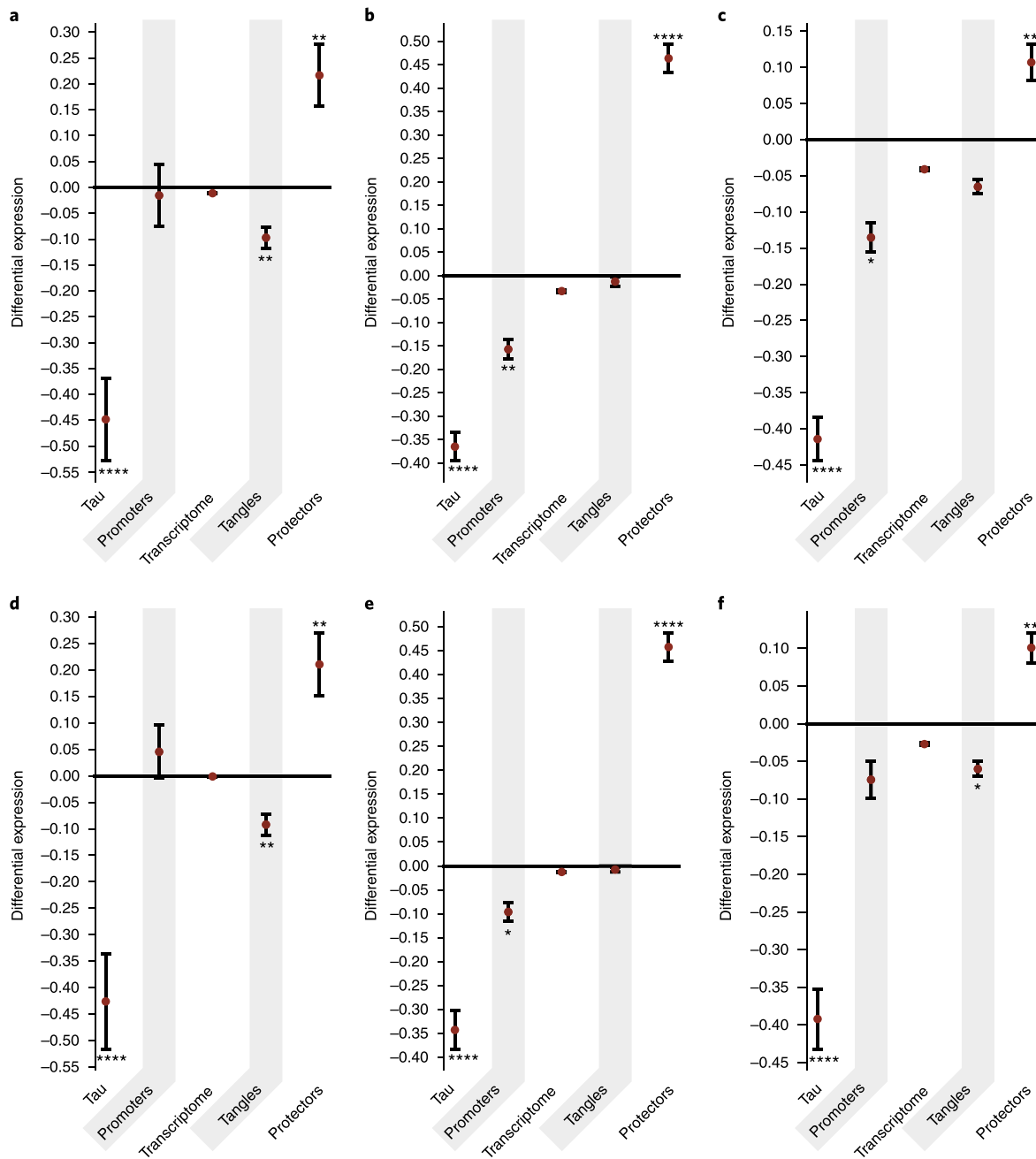
**Fig. 3 | Single-nucleus RNA-seq analysis reveals a specific tau homeostasis signature in EX neurons in human brains. a,b**, Comparison of the differential expression of relevant subproteomes for different cell types. For each subproteome (and the whole transcriptome as a control), the difference between the mean expression in EX and IN neurons (measured by the Δ score; see Methods) was calculated, and the values are presented as mean ± s.e.m. Results are reported for the SNS and the DroNc-Seq datasets, respectively. **c,d**, Comparison of Δ scores for five subproteomes (and the whole transcriptome as a control) within the EX neurons, between regions affected relatively early or late in AD for the SNS and DroNc-Seq datasets, respectively. Significance was evaluated by building a null model for each subproteome (see Methods, Supplementary Table 1, and Supplementary Figs. 4–6) and corrected with a Benjamini–Hochberg multiple-hypothesis-testing correction (*$P < 0.05$, **$P < 0.01$, ***$P < 0.001$, ****$P < 0.0001$). Subproteomes ($n_{sns}$ and $n_{drnc}$ are the sample sizes for SNS and DroNc-Seq datasets, respectively: EX markers, $n_{sns} = n_{drnc} = 2$; promoters, $n_{sns} = n_{drnc} = 6$; MS (a subset of highly expressed and aggregation-prone proteins, which are supersaturated—i.e., proteins whose concentration in the cellular environment is higher than a critical value keeping them soluble and functional—and downregulated in AD):, $n_{sns} = 162$, $n_{drnc} = 179$; whole transcriptome (here reported as a negative control); tangles (proteins co-aggregating with tau and found in neurofibrillary tangles), $n_{sns} = 57$, $n_{drnc} = 68$; protectors, $n_{sns} = n_{drnc} = 6$; IN markers, $n_{sns} = n_{drnc} = 3$).

loss of EX neurons was not associated with aging but with the maturation of tau pathology in the MEC. The increased number of MC1$^+$ neurons in the PRH and NC of EC-tau mice at 30+ months (Fig. 1e) indicates that the propagation and spreading of tau pathology from the primary to the secondary affected areas of the neocortex. Taken together, these results demonstrate that EX neurons are vulnerable to both the accumulation and the propagation of tauopathy in this mouse model of tauopathy.

**EX and IN human neurons are differentially vulnerable to tau pathology in primary and secondary affected regions of AD brain.** To explore whether or not pathological tau also differentially impacts human EX neurons in AD, we performed co-localization studies on postmortem brain tissues at different stages of AD, as assessed by the Braak staging protocol[4]. Consistent with the mouse data, we found that MC1$^+$ tau pathology was mainly co-localized with EX neuronal markers, but not IN neurons in layers II–IV of the EC and in secondary affected regions such as the prefrontal cortex (Brodmann area 9, BA9) at early and late Braak stages (Fig. 2a–c and Supplementary Fig. 2). Moreover, the numbers of EX neurons

were significantly reduced in the mid- to late-stage AD brain (Braak stages III–IV and V–VI) compared with non-AD controls (Braak stages I–II; Fig. 2d,e). Tau pathology was not evident in microglia (IBA1$^+$) or astrocytes (GFAP$^+$). The co-localization of pathological forms of tau with neuronal markers in both EC-tau mice and human AD was further confirmed with phosphorylation-site-specific tau antibodies. Consistent with the MC1 data, we found that EX neurons (SATB2$^+$), but not IN neurons (GAD1$^+$), co-localized with phospho-tau-specific antibodies, including AT8 (Ser202–Thr205), PHF1 (Ser396–Ser404), pS422-Tau (Ser422), and AT100 (Thr212–Ser214; Supplementary Fig. 3). Overall, these data suggest that in human brains, EX and IN neurons are differentially vulnerable to tau pathology in primary and secondary affected regions in AD. This conclusion is also consistent with previous reports of the selective vulnerability of pyramidal neurons in AD[4,6,12].

**Single-nucleus RNA-seq analysis reveals a specific tau homeostasis signature in EX neurons in the human brain.** We hypothesized that the selective vulnerability of EX neurons to tau pathology could be determined by an intrinsic difference in the cellular environment

**Fig. 4 | Single-nucleus RNA-seq analysis shows high levels of tau aggregation protectors in glia.** Differential expression of relevant subproteomes for different cell types. For each subproteome (and the transcriptome of reference as a control) the difference between the mean expression in glia and neurons (measured by the Δ score; see Methods), within cell-types from different regions was calculated. **a–c**, Differential expression values between glia and EX neurons are reported. Specifically, results are reported for (**a**) microglia (MG), (**b**) astrocytes (ASC1, ASC2), and (**c**) oligodendrocytes (ODC1, ODC2). **d–f**, Differential expression between glia and IN neurons are reported, with values corresponding to (**d**) microglia (MG), (**e**) astrocytes (ASC1, ASC2), and (**f**) oligodendrocytes (ODC1, ODC2). For each bar, the significance was evaluated by building a null model for each subproteome and corrected with a Benjamini–Hochberg multiple hypothesis testing correction; *$P < 0.05$, **$P < 0.01$, ****$P < 0.0001$ (see Methods, Supplementary Table 2, and Supplementary Figs. 8–10). Results are reported for the DroNc-Seq dataset. Subproteomes: tau (*MAPT*); sample sizes are as in Fig. 3.

in terms of the specific branch of the protein homeostasis system that regulates tau aggregation. To test this idea and to begin to identify this 'tau homeostasis system', we analyzed two independent single-nucleus RNA-seq datasets (SNS and DroNc-Seq) obtained from postmortem brain tissues of healthy adults without AD pathology[24,25]. We found that the mRNA levels of genes encoding the proteins making up a metastable subproteome (MS)[26], tau co-aggregators, and tau aggregation promoters[19] were increased, but the

mRNA levels of tau aggregation protector genes[19] were decreased in EX neurons compared with IN neurons. Furthermore, differential expression of the tau homeostasis genes was seen in regions affected early (BA21, including EC; BA22, BA10, and BA41; and hippocampus) and late (BA17 and BA9) in AD (Fig. 3a–d, Supplementary Table 1, and Supplementary Figs. 4 and 5). Overall, a statistically significant and consistent pattern emerged from the analysis of the two datasets, indicating that genes encoding proteins involved in

tau homeostasis (tau aggregation promoters and protectors and tau co-aggregators) and proteins in the MS were differentially regulated in cells that are vulnerable to tauopathy compared to those that are resistant to it. Taken together (Supplementary Fig. 6), these results indicate that dysregulated tau homeostasis is closely linked to the etiology of tauopathy.

**Glial cells have higher levels of aggregation protectors than neurons.** We observed that the subproteomes most relevant to tau homeostasis showed a specific signature for neurons compared to glial cell types (microglia, oligodendrocytes, and astrocytes). Overall, we observed statistically significant increases in mRNA levels of genes protecting from tau aggregation in glia cells, combined with relatively low expression of tau and low mRNA levels of genes promoting tau aggregation and encoding its co-aggregators (Fig. 4 and Supplementary Table 2). These data were consistent with the observation that glia cells in the AD brain did not accumulate detectable levels of pathological tau (Supplementary Fig. 2).

***BAG3* is a hub gene in the co-expression network relevant to tau homeostasis.** To identify a key master regulator responsible for modulating tau aggregates among the subproteomes linked to tau homeostasis, we performed a co-expression network analysis[27] on the SNS dataset. This type of analysis quantifies the covariation of genes within given samples or brain regions (cell types in our case) by measuring a quantity of reference, such as the Pearson's correlation coefficient. In this network, each gene is represented by a node and the co-expression values correspond to the weights associated with each link connecting two nodes. Although more complex approaches are possible[27], a direct way to identify the hub genes that are central in the network is to sum the weights of all the links connected to a gene, which is defined as the total degree of a node. When the top 10% of the genes in the higher degree were isolated (Fig. 5), the only gene belonging to both the protector subproteome and to the top 10% of the most co-expressed genes was *BAG3*. All the other genes belonged either to the MS or to the tangles, and no gene belonging to the promoter group was found among the hub genes (Supplementary Table 3).

**Validation of the localization and expression levels of representative tau homeostasis signature genes by single-molecule FISH in human EC and prefrontal cortex.** We next validated the results of the single-nucleus RNA-seq analysis of several AD-related genes, including *MAPK1* (tau co-aggregators), *FKBP5* (tau aggregation promoter), *ENC1* (MS), and *MAPT* (the gene encoding tau) using a single-molecule RNA fluorescence in situ hybridization assay. The mRNA levels of *MAPK1*, *FKBP5*, and *ENC1* were significantly higher in EX neurons than in IN neurons in both EC and BA9, while there was no significant difference in the mRNA levels corresponding to *MAPT* (Fig. 6). These results support the conclusion that in vulnerable regions, EX neurons exhibit a cellular environment more conducive to tau aggregation and susceptibility to tau homeostasis dysfunction than IN neurons.

**Validation of BAG3 protein levels in IN neurons and EX neurons of unaffected and AD brain tissue.** To validate whether the protein level of one of the genes identified by the RNA analysis was differentially regulated between IN and EX neurons, and whether this was seen in both unaffected (non-AD) and AD brains, we examined the levels of BAG3 by immunofluorescence staining in the BA9 region of postmortem human tissue. BAG3 levels in NeuN^{+} neurons labeled with the IN cell marker GAD1 (GAD1^{+}NeuN[+]) were significantly higher in both non-AD and in AD neurons than in GAD[−]NeuN^{+} neurons ($P < 0.001$, Supplementary Fig. 7). These cells were presumed to be mostly EX, as the great majority of GAD[−]NeuN^{+} neurons co-labeled with EX neuron markers (data not shown).
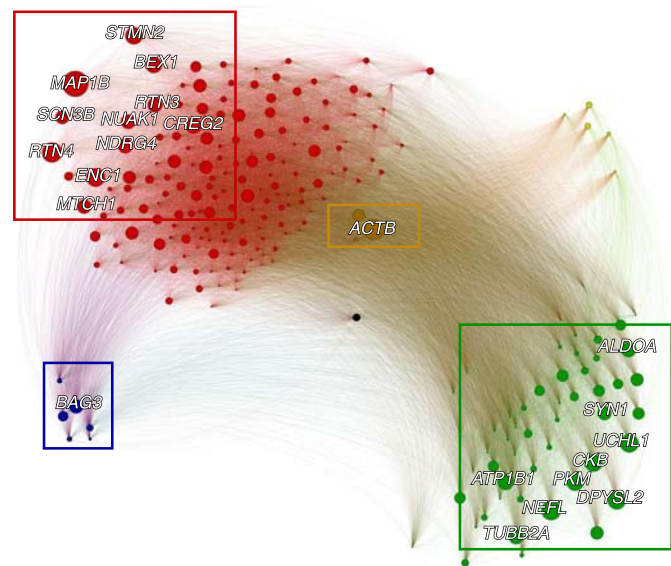


**Fig. 5 | Co-expression network analysis of the subproteomes relevant to tau homeostasis.** Sketch of the co-expression network to identify hub genes of the subproteomes related to tau homeostasis. The network is fully connected, and the edges linking the genes (nodes) are weighted with the Pearson's correlation coefficient. The hubs, which are defined as the genes more tightly co-expressed with every other gene in the network (and here defined as master regulators), are highlighted with the labels (top 10% of the most co-expressed genes). The size of each node is proportional to the sum of the weights of the edges connected to it. *BAG3* is a hub in the protectors region of the network (lower left). Colors identify different subproteomes: MS (red), tangles (green), protectors (blue), promoters (yellow), tau (black), and genes shared between MS and tangles (brown).

Of note, the level of BAG3 protein was much higher in non-neuronal cells (NeuN^{−} cells) than in neurons (NeuN^{+} cells; Supplementary Fig. 7a). These results are consistent with our findings of almost no accumulation of pathological tau in IN neurons and glial cells.

**Modulating the expression of BAG3 affects tau accumulation in primary cortical neurons.** To further validate our results and confirm that genes identified through the bioinformatics analysis can contribute to the vulnerability of neurons to tauopathy, we manipulated the mRNA levels of *BAG3*, a master regulator gene and one of the major tau aggregation protectors associated with tau homeostasis[21] that was enriched in inhibitory neurons (Supplementary Table 1). BAG3 was of particular interest as it interacts with the co-chaperone HSPB8, which was also more highly expressed in IN neurons than in EX neurons (Supplementary Table 1). We found that knockdown of BAG3 using short hairpin RNA (shRNA) lentivirus in primary neurons from wild-type mice (Fig. 7a and Supplementary Fig. 11) induced accumulations of endogenous tau recognized by the 12E8 antibody, mainly in neurites (Fig. 7b,c; $P < 0.01$). In primary neurons expressing tau RD-P301S-YFP (an FTLD-causing mutation), knockdown of BAG3 led to an accumulation of tau in both cell bodies and neurites (Fig. 7d–f; $P < 0.01$). Overexpression of BAG3 significantly attenuated tau accumulation in EX neurons (Fig. 7d,e; $P < 0.01$). There was a trend toward decreased tau accumulation in IN neurons where BAG3 was overexpressed, but the data did not reach significance (Fig. 7f; $P = 0.098$), most likely due to the very low level of tau aggregates in IN neurons in general. These results support our conclusion that genes associated with tau protein homeostasis contribute to neuronal vulnerability to tau pathology.
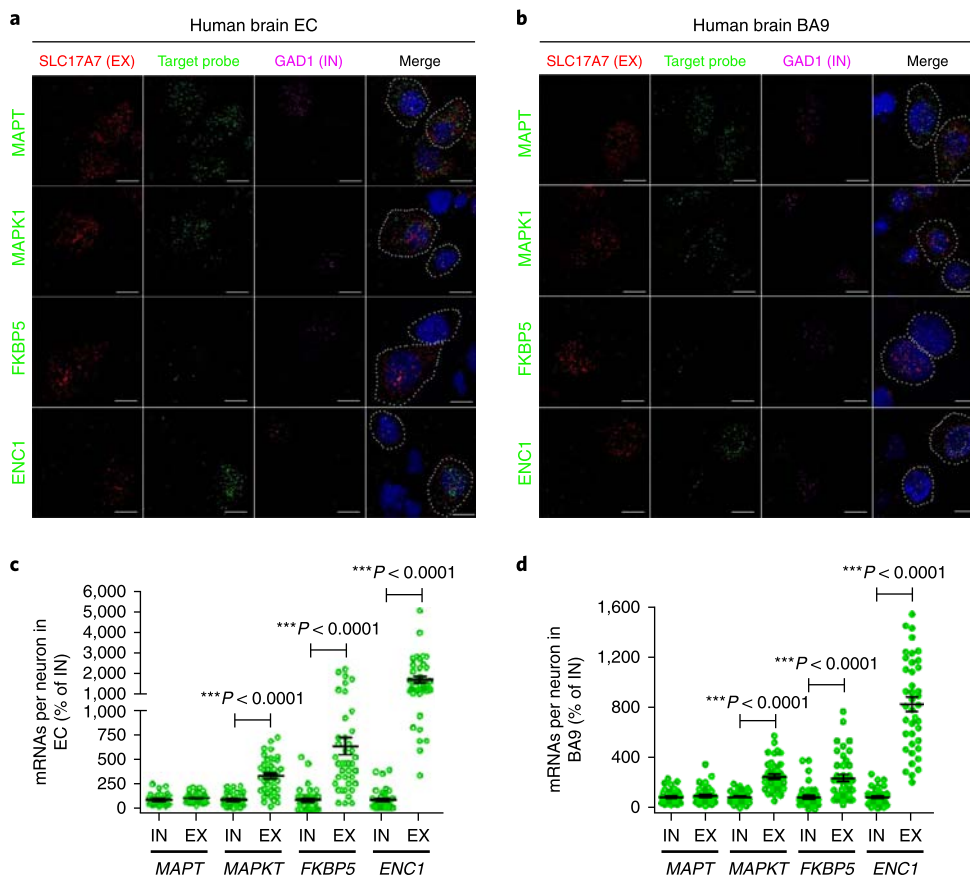
**Fig. 6 | Validation by single-molecule fluorescence in situ hybridization of the localization and mRNA expression levels of representative tau homeostasis signature genes in human EC and prefrontal cortex. a,b**, Representative single-molecule fluorescence in situ hybridization (sm)-FISH images of the co-staining of EX neuronal marker (*SLC17A7*, red), IN neuronal marker (*GAD1*, purple), and target probe (*MAPT*, *MAPK1*, *FKBP5*, and *ENC1*; green) in the (**a**) EC and (**b**) BA9 of human brain without pathological hallmarks of neurodegenerative diseases (54–66 years old); dotted ovals represent individual EX or IN neurons. Three independent experiments were repeated with similar results. Scale bar, 10 μm. **c,d**, Comparison of the number of single RNAs of the target probe in individual EX and IN neurons in (**c**) EC (two-tailed unpaired *t* test with Welch's correction; ***$P < 0.0001$ vs. IN neurons; $t_{47} = 8.061$, $t_{42} = 6.181$, $t_{39} = 10.77$) and (**d**) BA9 regions (two-tailed unpaired *t* test with Welch's correction; ***$P < 0.0001$ vs. IN neurons; $t_{48} = 7.981$, $t_{56} = 4.675$, $t_{41} = 12.60$). Data are presented as mean ± s.e.m.; $n = 4$ human brains, 10 neurons per brain.

## Discussion

Understanding the molecular origins of selective cellular vulnerability is of fundamental importance for all neurodegenerative diseases[28]. Unfortunately, the molecular determinants of selective vulnerability have so far remained unclear, in part because we lack sufficient information on the molecular makeup of subpopulations of cells that are compromised in a particular brain region, by a particular protein, and in a particular disease. In this study, we addressed this problem with regard to tau using a mouse model of tauopathy, as well as human AD brains at different Braak stages. The EC-tau mouse model[20,29] demonstrates progressive tauopathy that originates in the hippocampal formation but spreads to extrahippocampal and neocortical areas with age[30]. Because the model showed spread of the pathology, we were able to dissociate primary vulnerability from secondary vulnerability that occurred as a result of non-cell-autonomous tauopathy propagation. Primary vulnerability was seen in MEC neurons, which developed tau pathology early, whereas secondary vulnerability was seen in PRH and NC neurons, which developed pathology much later. We demonstrated that tau aggregates predominantly accumulated in EX neurons compared to IN neurons, not only in the primary affected region but also in secondary regions, suggesting that EX neurons were vulnerable to both cell autonomous and non-cell-autonomous accumulations of tau as tauopathy propagates.

Previous studies have explored why putative EX neurons could be particularly vulnerable to degeneration in AD and other neurodegenerative disorders[6,13–15]. However, mechanisms underlying selective vulnerability of EX neurons to tau pathology have not been identified and tested. Our approach to answering this question was prompted by recent observations that age-related stress and dysfunction of protein homeostasis are observable in vulnerable neurons in aging and age-related neurodegenerative diseases[14,16–18]. In particular, a transcriptional analysis of healthy brains at ages well before the typical onset of AD identified a protein homeostasis signature associated with protein aggregation and predicted the Braak staging of AD[19]. The protein homeostasis signature included a set of aggregation-prone proteins (MS)[26] and three other sets of protein homeostasis components (co-aggregators, aggregation promoters, and aggregation protectors)[18]. The overall relative expression of the protein homeostasis signature was elevated substantially in neurons compared with other cell types, indicating that neurons have a cellular environment most conducive to protein aggregation compared to other brain cell types[19].

Based on these results, we hypothesized that an intrinsic difference in the tau homeostasis system could contribute to the selective vulnerability of EX neurons to tau pathology. After analyzing two independent single-nucleus RNA-seq datasets from healthy donors, we showed that EX neurons are characterized by elevated expression
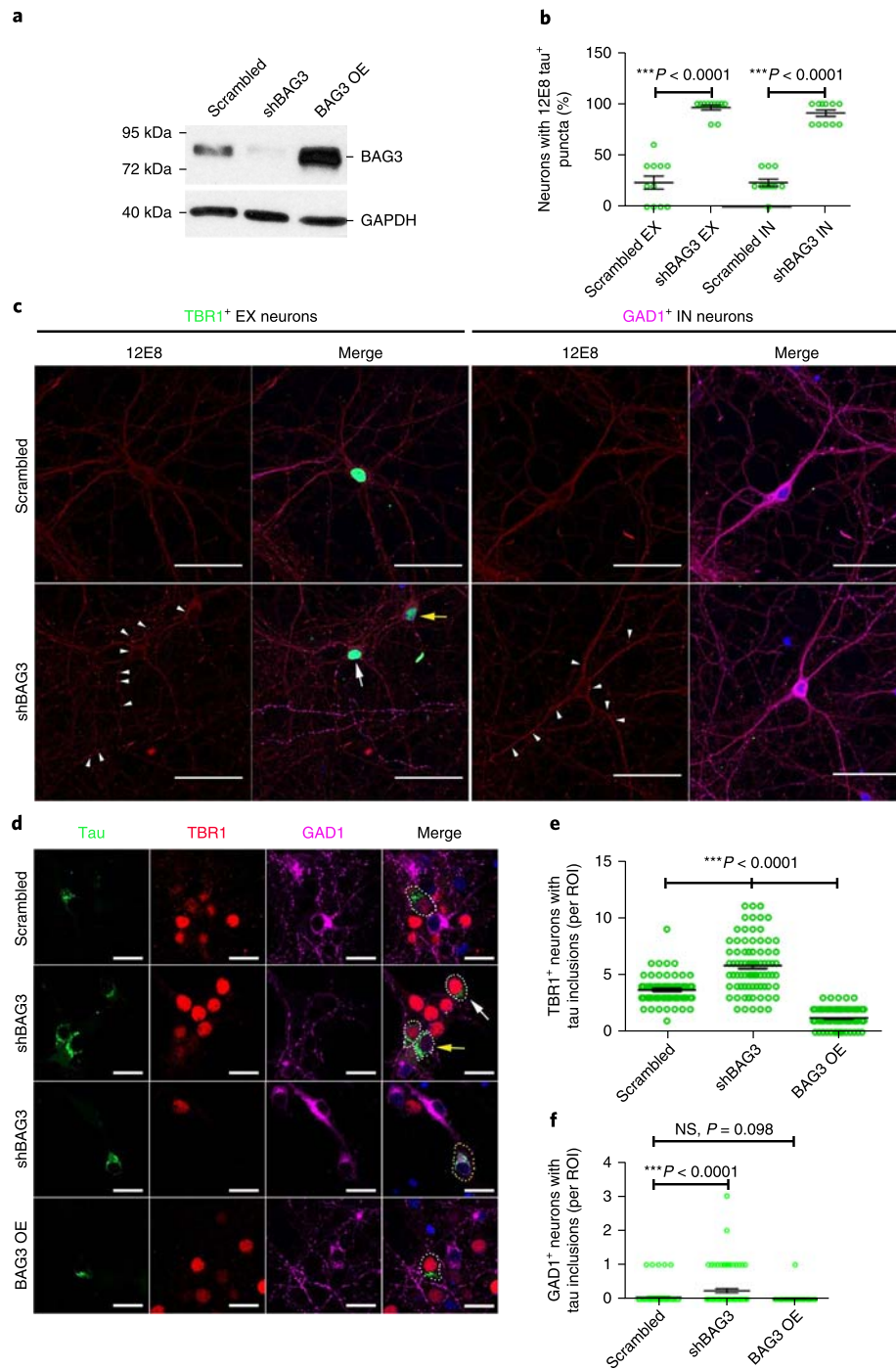
**Fig. 7 | Modulating the expression of one of the tau aggregation protectors, BAG3, affects tau accumulation in primary cortical neurons.**
**a**, Representative western blot images of primary cortical neurons transduced with lentivirus expressing scrambled BAG3, short hairpin BAG3 (shBAG3), or overexpressed BAG3 (OE), as described in Methods. GAPDH is a housekeeping protein used as the loading control. Three independent experiments were repeated with similar results. Full length blots can be found in Supplementary Fig. 11. **b**, The percentages of EX and IN neurons ($n = 55$ from 11 coverslips per group) with 12E8 (pS262 and/or pS356 tau)-positive puncta ($\geq 5$) in the neurites were quantified as described in Methods (data are presented as mean ± s.e.m.; nonparametric Kruskal–Wallis test with Dunn's post hoc multiple-comparisons test; ***$P < 0.0001$ vs. neurons transduced with scrambled BAG3; Kruskal–Wallis statistic = 34.54). **c**, Representative immunocytochemical images of 12E8+ (red) puncta (white arrowheads) in the neurites of TBR1+ (green) EX neurons. White arrow, neuron with high TBR1; yellow arrow, neuron with low TBR1. GAD1+ (purple) IN neurons were also transduced with shBAG3 and tau was shown to accumulate in neurites (white arrowheads). Three independent experiments were repeated with similar results. Scale bars, 50 μm. **d**, Representative immunocytochemical images of tau inclusions (green) in TBR1+ (red) EX neurons (white dotted circle) and tau inclusions (green) in GAD1+ (purple) IN neurons (yellow dotted circle) transduced with different lentiviruses as described in Methods. White arrow, high TBR1; yellow arrow, low TBR1. Nuclei were counterstained with Hoechst33342 (blue). Three independent experiments were repeated with similar results. Scale bars, 20 μm. **e,f**, Quantitation of numbers of TBR1+ EX and GAD1+ IN neurons with tau inclusions ($n = 80$ region of interests (ROIs) from 4 coverslips per group; data are presented as mean ± s.e.m.; nonparametric Kruskal–Wallis tests with Dunn's post hoc multiple-comparisons tests; ***$P < 0.0001$ vs. neurons transduced with scrambled BAG3; Kruskal–Wallis statistics: (**e**) 164.6 and (**f**) 20.09).

of a specific subset of aggregation-prone proteins (the MS) and tau aggregation promoters, as well as by decreased expression of tau aggregation protectors. These findings suggest that the selective vulnerability of EX neurons to tau aggregation, particularly in regions of the brain that are affected early on in AD, could be due to the intrinsic susceptibility of EX neurons to dysregulation of the branch of the protein homeostasis system that regulates tau aggregation. Since there are currently only two publicly available single-nuclei RNA-seq datasets from postmortem human brain tissue and they do not contain the exact same regions of the brain, we could not compare region-matched datasets. However, we still found that tau homeostasis gene signatures differed between EX and IN neurons in early and late affected region, even though the regions considered were not the same.

This idea is supported by the finding of relatively high expression of tau aggregation protectors in IN neurons and other cell types, such as microglia, that are resistant to pathological tau accumulation, in agreement with previous findings[19]. Differential regulation of several of the genes was validated at the mRNA level, and the protein level of *BAG3*, a master regulator belonging both to the 'protectors' subproteome and to the top 10% of most co-expressed genes, was shown to be substantially higher in IN neurons than in putative EX (GAD⁻NeuN⁺) neurons in both non-AD and AD cases, supporting our finding that tau did not accumulate in IN neurons in AD brains. Furthermore, when we attenuated the level of BAG3 in primary neurons, the vulnerability of the cells to tau accumulation was substantially enhanced. As the promoter used to drive expression of the *BAG3* shRNA or cDNA is not specific for neuron types, *BAG3* mRNA was modulated in both EX and IN neurons. We expected the levels of tau to be attenuated in both EX and IN neurons in response, as our RNA data had shown that the gene is differentially, not selectively, regulated between the two neuron types, but it was noteworthy to observe that when BAG3 expression was reduced, tau accumulated in GAD⁺ IN neurons. We have only very rarely observed tau accumulating in IN neurons in mouse or human studies. Conversely, vulnerability was reduced in neurons when BAG3 was overexpressed. These data confirm that the gene was impactful in IN neurons.

Our results indicate that neurons (and EX neurons in particular) represent a cellular environment more vulnerable to pathological tau accumulation compared to glial cell types, which is consistent with the finding that tau does not accumulate appreciably in glia in the AD brain. However, tau has been shown to accumulate in glia (tufted astrocytes and oligodendrocytes) in some but not all of the primary tauopathies[31–33]. Why tau should accumulate in glia in some tauopathies is not known, but from our results we suggest that it likely results from a combination of different forms of tau in different tauopathies and the sets of homeostasis genes in each cell type that control their likelihood to accumulate.

Our results are consistent with the known effects of impaired protein homeostasis on pathogenesis in age-related neurodegenerative diseases[14,16–18]. Our findings characterize a subset of proteins that are highly specific for tau homeostasis, and they complement previous studies on protein subnetworks responsible for protein homeostasis in different neurodegenerative disorders[34]. We anticipate that further demonstrations of the complex and highly regulated interactions between different protein homeostasis components will reveal more determinants of the vulnerability of specific neuron types. Lastly, our findings emphasize the importance of pursuing novel therapeutic strategies of enhancing natural defense mechanisms that maintain our proteome in a soluble state[35,36] and the use of protein homeostasis enhancing therapeutics, especially if they can be designed to target specific cell types, such as vulnerable EX neurons.

## Online content

Any methods, additional references, Nature Research reporting summaries, source data, statements of data availability and associated accession codes are available at https://doi.org/10.1038/s41593-018-0298-7.

## References

1. Šimić, G. et al. Tau protein hyperphosphorylation and aggregation in Alzheimer's disease and other tauopathies, and possible neuroprotective strategies. *Biomolecules* **6**, 6 (2016).
2. Dugger, B. N. & Dickson, D. W. Pathology of neurodegenerative diseases. *Cold Spring Harb. Perspect. Biol.* **9**, a028035 (2017).
3. Spina, S. et al. The tauopathy associated with mutation+3 in intron 10 of Tau: characterization of the MSTD family. *Brain* **131**, 72–89 (2008).
4. Braak, H. & Braak, E. Neuropathological stageing of Alzheimer-related changes. *Acta Neuropathol.* **82**, 239–259 (1991).
5. Davies, P. & Maloney, A. J. Selective loss of central cholinergic neurons in Alzheimer's disease. *Lancet* **2**, 1403 (1976).
6. Morrison, B. M., Hof, P. R. & Morrison, J. H. Determinants of neuronal vulnerability in neurodegenerative diseases. *Ann. Neurol.* **44**(Suppl 1), S32–S44 (1998).
7. Götz, J., Schonrock, N., Vissel, B. & Ittner, L. M. Alzheimer's disease selective vulnerability and modeling in transgenic mice. *J. Alzheimers Dis.* **18**, 243–251 (2009).
8. Riascos, D. et al. Age-related loss of calcium buffering and selective neuronal vulnerability in Alzheimer's disease. *Acta Neuropathol.* **122**, 565–576 (2011).
9. Ahmadian, S. S. et al. Loss of calbindin-D28K is associated with the full range of tangle pathology within basal forebrain cholinergic neurons in Alzheimer's disease. *Neurobiol. Aging* **36**, 3163–3170 (2015).
10. Hof, P. R. et al. Age-related distribution of neuropathologic changes in the cerebral cortex of patients with Down's syndrome. Quantitative regional analysis and comparison with Alzheimer's disease. *Arch. Neurol.* **52**, 379–391 (1995).
11. Seeley, W. W. Selective functional, regional, and neuronal vulnerability in frontotemporal dementia. *Curr. Opin. Neurol.* **21**, 701–707 (2008).
12. Hyman, B. T., Van Hoesen, G. W., Damasio, A. R. & Barnes, C. L. Alzheimer's disease: cell-specific pathology isolates the hippocampal formation. *Science* **225**, 1168–1170 (1984).
13. Mattson, M. P. & Magnus, T. Ageing and neuronal vulnerability. *Nat. Rev. Neurosci.* **7**, 278–294 (2006).
14. Saxena, S. & Caroni, P. Selective neuronal vulnerability in neurodegenerative diseases: from stressor thresholds to degeneration. *Neuron* **71**, 35–48 (2011).
15. Roselli, F. & Caroni, P. From intrinsic firing properties to selective neuronal vulnerability in neurodegenerative diseases. *Neuron* **85**, 901–910 (2015).
16. Labbadia, J. & Morimoto, R. I. The biology of proteostasis in aging and disease. *Annu. Rev. Biochem.* **84**, 435–464 (2015).
17. Taylor, R. C. & Dillin, A. Aging as an event of proteostasis collapse. *Cold Spring Harb. Perspect. Biol.* **3**, a004440 (2011).
18. Kaushik, S. & Cuervo, A. M. Proteostasis and aging. *Nat. Med.* **21**, 1406–1415 (2015).
19. Freer, R. et al. A protein homeostasis signature in healthy brains recapitulates tissue vulnerability to Alzheimer's disease. *Sci. Adv.* **2**, e1600947 (2016).
20. Liu, L. et al. Trans-synaptic spread of tau pathology in vivo. *PLoS One* **7**, e31302 (2012).
21. Lei, Z., Brizzee, C. & Johnson, G. V. BAG3 facilitates the clearance of endogenous tau in primary neurons. *Neurobiol. Aging* **36**, 241–248 (2015).
22. Seidel, K. et al. The HSPB8-BAG3 chaperone complex is upregulated in astrocytes in the human brain affected by protein aggregation diseases. *Neuropathol. Appl. Neurobiol.* **38**, 39–53 (2012).
23. Wegmann, S. et al. Removing endogenous tau does not prevent tau propagation yet reduces its neurotoxicity. *EMBO J.* **34**, 3028–3041 (2015).
24. Lake, B. B. et al. Neuronal subtypes and diversity revealed by single-nucleus RNA sequencing of the human brain. *Science* **352**, 1586–1590 (2016).
25. Habib, N. et al. Massively parallel single-nucleus RNA-seq with DroNc-Seq. *Nat. Methods* **14**, 955–958 (2017).
26. Ciryam, P. et al. A transcriptional signature of Alzheimer's disease is associated with a metastable subproteome at risk for aggregation. *Proc. Natl Acad. Sci. USA* **113**, 4753–4758 (2016).
27. Zhang, B. & Horvath, S. A general framework for weighted gene co-expression network analysis. *Stat. Appl. Genet. Mol. Biol.* **4**, e17 (2005).
28. Fu, H., Hardy, J. & Duff, K. E. Selective vulnerability in neurodegenerative diseases. *Nat. Neurosci.* **21**, 1350–1358 (2018).
29. de Calignon, A. et al. Propagation of tau pathology in a model of early Alzheimer's disease. *Neuron* **73**, 685–697 (2012).
30. Fu, H. et al. 3D visualization of the temporal and spatial spread of tau pathology reveals extensive sites of tau accumulation associated with neuronal loss and recognition memory deficit in aged tau transgenic mice. *PLoS One* **11**, e0159463 (2016).

31. Ferrer, I. et al. Glial and neuronal tau pathology in tauopathies: characterization of disease-specific phenotypes and tau pathology progression. *J. Neuropathol. Exp. Neurol.* **73**, 81–97 (2014).
32. Kahlson, M. A. & Colodner, K. J. Glial tau pathology in tauopathies: functional consequences. *J. Exp. Neurosci.* **9**(Suppl 2), 43–50 (2016).
33. Leyns, C. E. G. & Holtzman, D. M. Glial contributions to neurodegeneration in tauopathies. *Mol. Neurodegener.* **12**, 50 (2017).
34. Brehme, M. et al. A chaperome subnetwork safeguards proteostasis in aging and neurodegenerative disease. *Cell Rep.* **9**, 1135–1150 (2014).
35. Baranczak, A. & Kelly, J. W. A current pharmacologic agent versus the promise of next generation therapeutics to ameliorate protein misfolding and/ or aggregation diseases. *Curr. Opin. Chem. Biol.* **32**, 10–21 (2016).
36. Balch, W. E., Morimoto, R. I., Dillin, A. & Kelly, J. W. Adapting proteostasis for disease intervention. *Science* **319**, 916–919 (2008).

## Author contributions

K.E.D., H.F., and M.V. jointly designed and supervised the study, discussed the results, and wrote the paper. H.F. designed and performed experiments and analyzed the data. A.P., R.F., and M.V. analyzed single-nucleus RNA-seq datasets. A.P. discussed the results and wrote parts of the paper. Y.N., N.C.H.V., M.T., P.V.M.C., B.A.L., S.L.F., S.C., and H.Y.F. provided technical assistance. E.D.H. provided critical input into the paper. G.V.W.J. designed and supplied all the BAG3-related viruses. All authors discussed the results and contributed to the manuscript.

## Competing interests

K.E.D. is on the board of directors and SAB of Ceracuity LLC. All other authors declare no competing interests.

## Additional information

**Supplementary information** is available for this paper at https://doi.org/10.1038/s41593-018-0298-7.

**Reprints and permissions information** is available at www.nature.com/reprints.

**Correspondence and requests for materials** should be addressed to H.F. or M.V. or K.E.D.

**Publisher's note:** Springer Nature remains neutral with regard to jurisdictional claims in published maps and institutional affiliations.

## Methods

**Reagents.** Human conformation-dependent tau (MC1) and human/murine phospho-tau pSer396/ Ser404 (PHF1) monoclonal antibodies were provided by P. Davies. Mouse anti-phosphorylated tau Ser262 and/or Ser356 (12E8) antibodies[37] were provided by P. Dolan. Human/murine phospho-tau pSer202/Thr205 (AT8, Cat# MN1020) and pThr212/Ser214 (AT100, Cat# MN1060) monoclonal antibodies, rabbit anti-phospho-tau pSer422 (pS422, Cat# 44-764 G), and parvalbumin (PVALB, Cat# PA5-18389) polyclonal antibodies, Alexa Fluor dye-labeled goat and donkey secondary antibodies (Cat# A-11029, A-11037, A-11007, A-11058, and A-21202), SlowFade gold (Cat# S36937), and ProLong gold (Cat# P36934) antifade reagents were purchased from Thermo Fisher Scientific. Rabbit anti-TBR1 (Cat# ab31940) and SATB2 (Cat# ab92446) polyclonal antibodies were purchased from Abcam. Rat anti-somatostatin (SST; Cat# MAB354) and mouse anti-NeuN (Cat# MAB377) monoclonal antibody and goat anti-GAD1 (Cat# AF2086) polyclonal antibody were purchased from Millipore and R&D Systems, respectively. Rabbit anti-calretinin (CALB2; Cat# 7697), IBA-1 (Cat# 019-19741), and GFAP (Cat# G9269) polyclonal antibodies were purchased from Swant, Wako, and Sigma-Aldrich, respectively. RNAscope Multiplex Fluorescence Kit (Cat #320851) and human-specific RNA probes, including *SLC17A7* (Cat# 415611 or 415611-C2), *GAD1* (Cat# 404031-C3), *MAPT* (Cat# 472621), *MAPK1* (Cat# 470741), *FKBP5* (Cat# 481101), and *ENC1* (custom probe), were purchased from Advanced Cell Diagnostics. TrueBlack lipofuscin autofluorescence quencher (Cat# 23007) was purchased from Biotium. Lentiviral vectors FG12-scramble and FG12-shBAG3 were prepared as previously described[21], and the GFP in these vectors was removed by cutting with AgeI and BsrGI followed by fill-in of 5′ overhangs and re-ligation. The shRNA-resistant *BAG3* in FigB was made by changing the underlined bases of the shRNA target sequence (A<u>A</u>G <u>G</u>TT <u>C</u>AG <u>A</u>CC ATC TTG GAA), which does not change the amino acid but results in an shRNA-resistant *BAG3* (AAA GTA CAA ACT ATC TTG GAA). Viral packaging vectors *psPAX2* and *VSVG* were provided by C. Pröschel. Tau RD-P301S-YFP (aa 244–372 of the 441 amino acids in full-length tau; mutations P301S) and the clone 9 (DS9) tau seeds (provided by M. Diamond) were prepared as previously described[38]. Rabbit anti-TBR1 (Cat# 20932-1-AP) and rabbit anti-BAG3 (Cat# 10599-1-AP) polyclonal antibody were purchased from Proteintech Group. Unless otherwise noted, all other reagents were purchased from Fisher Scientific or Thermo Fisher Scientific.

**Animals.** We previously generated a tau transgenic mouse model known as EC-tau[20] by crossing the neuropsin-tTA activator line with a tetracycline-inducible tau P301L responder line. The F1 offspring (both males and females at 22 and 30+ months old, strain FVB/N:C57BL/6) were used as experimental animals. All animals were maintained on a 12-h light/dark cycle with food and water provided ad libitum. All animal experiments were performed in accordance with national guidelines (National Institutes of Health) and approved by the Institutional Animal Care and Use Committee of Columbia University. Mice were transcardially perfused with phosphate-buffered saline (PBS), brains were harvested and drop-fixed in 4% paraformaldehyde (PFA; Cat# 15710, Electron Microscopy Sciences) in PBS at 4 °C overnight, and free-floating sections (35 μm) were prepared as previously described[39].

**Human brain tissues.** Human free-floating sections (40 μm) and formalin-fixed paraffin-embedded (FFPE) sections (10 μm) were provided by the Brain Bank at Banner Sun Health Research Institute. Human fresh-frozen brain blocks were provided by the New York Brain Bank at Columbia University Medical Center and the NIH NeuroBrainBank at the University of Maryland Brain and Tissue Bank. The demographics of human cases used in this study are listed in Supplementary Table 4. These specimens were obtained by consent at autopsy and have been de-identified and are IRB exempt so as to protect the identity of each patient. Frozen sections (10 μm) were cut from frozen blocks under RNase-free conditions by the Histology Service at Columbia University Medical Center.

**Immunofluorescence staining on mouse and human brain sections.** Immunostaining was performed as previously described with a few modifications for human brain sections[39]. Free-floating brain sections from EC-tau and age-matched nontransgenic (WT) mice at 22 and 30+ months as well as from human brains were subjected to antigen retrieval by 10-min incubation in 10 mM sodium citrate (pH 6.0, 95 °C). After blocking, the sections were stained with TBR1 (1:250), SATB2 (1:250), PVALB (1:1,000), SST (1:100), or CALB2 (1:1,000) antibodies in the blocking solution on the first day, followed by incubation with MC1 (1:750), AT8 (1:500), PHF1 (1:500), or pS422 (1:250) tau antibodies on the next day. Fresh-frozen human brain sections were air-dried and fixed with cold acetone for 10 min at −20 °C. They were then incubated with TBR1 (1:250), SATB2 (1:250), GAD1 (1:100) or GFAP (1:2,500) antibodies in blocking solution, followed by incubation with AT8 (1:500), PHF1 (1:500), pS422 (1:250) or AT100 (1:500) tau antibodies on the next day. Human FFPE sections were deparaffinized and rehydrated before the same procedure of antigen retrieval described above, followed by sequential immunolabeling with TBR1 (1:250), SATB2 (1:250) or IBA-1 (1:500) antibodies and MC1 or AT8 tau antibodies (1:500). We chose the sequential staining instead of the more common co-staining because we found substantial co-localization

artifacts of tau and neuronal markers, especially SST. After three washes with phosphate-buffered saline with Tween 20 solution (PBST), the sections were incubated with appropriate Alexa Fluor dye-labeled cross-absorbed goat or donkey secondary antibodies (1:1,000) for 2 h (mouse sections) or 3 h (human sections) at 20–25 °C. Following three washes with phosphate buffered saline solution (PBS), autofluorescence was quenched with 0.3% Sudan black in 70% ethanol for 6 min (mouse sections) or 12 min (human sections) at room temperature. The nuclei were stained with 5 mg/mL Hoechst33342 (Cat# 14533, Sigma-Aldrich) in PBST for 10 min at room temperature. Following three washes with PBS, sections were mounted on slides using SlowFade gold antifade reagent and imaged using confocal laser scanning microscopy (LSM800, Zeiss) via z-stack to assess co-localization. A fluorescence microscope (BX51, Olympus) was used for quantitation. The numbers of neuronal marker-positive, MC1+, and co-stained neurons in layers II–IV of the MEC, PRH, and NC were quantified manually using ImageJ software.

Co-staining GAD1 (1:100), NeuN (1:250), and BAG3 (1:100) on human brain frozen sections (BA9 region) was performed as described above. Stained sections were imaged using confocal laser scanning microscopy via z-stack. We used ImageJ to open the original CZI files, customize the channel colors, set measurements in analysis (mean intensity and area), and select different types of neurons by drawing a circle around the cell. The 'measure' function generated the analysis. The automatically generated values for similar-sized EX (GAD1⁻NeuN⁺) and IN (GAD1⁺NeuN⁺) neurons were used for comparison of the protein levels of BAG3.

**Single-nucleus RNA-seq data analysis.** We used two single-nucleus RNA-seq annotated datasets, SNS (http://genome-tech.ucsd.edu/public/Lake_Science_2016/)[24] and DroNc-Seq (https://portals.broadinstitute.org/single_cell)[25]. A differential expression analysis was performed on both datasets. Raw data were log-normalized, and then z-score normalization was performed for all genes across the samples to enable direct comparisons between them. Genes with replicates were first z-scored and then the averaged across different samples. For the DroNc-Seq dataset, the matrix of transcript reads had many zero entries within the transcriptome. To avoid biases in the analysis and reduce the amount of noise, the bottom 5% lowest-quality samples (samples with fewest reads across the transcriptome) were discarded, as they were considered to have been damaged during the experimental procedure. A Δ score[19] for the genes corresponding to each subproteome was calculated as $\Delta(\{s\}) = \bar{E}_{\{s\},\{i\}} - \bar{E}_{\{s\},\{j\}}$, which represents the difference between the average expression value ($\bar{E}$) computed, taking the subproteome {s} of reference, in the cell types {i} (for example, EX neurons), and {j} (for example, IN neurons), respectively. Cells were classified as either EX or IN neurons, or non-neuronal based on canonical marker gene expression. More specifically, cells were classified as EX neurons if the maximum expression of EX genes (*SLC17A6*, *SLC17A7*) was greater than the maximum expression of IN (*GAD1*, *GAD1*, *SLC32A1*) or non-neuronal (*OLIG1*, *GJA1*, *XDH*, *CTSS*, *MY19*) genes. Cells were classified as IN neurons if the maximum expression of IN (*GAD1*, *GAD1*, *SLC32A1*) genes was greater than the maximum expression of EX (*SLC17A6*, *SLC17A7*) or non-neuronal (*OLIG1*, *GJA1*, *XDH*, *CTSS*, *MY19*) genes. All remaining cells were classified as non-neuronal[40]. For the SNS dataset, we combined brain regions BA21, BA22, BA10, and BA41 and considered them to be a region affected early in AD (low Braak stage). BA17 was considered to be a region affected later in AD (higher Braak stage) region. For the DroNc-Seq dataset, hippocampus (HP) was considered to be an early-affected region, while the prefrontal cortex (PFC/BA9) was considered to be a later-affected region[4].

**Statistical analysis of the RNA-seq results.** The statistical significance of the results in Figs. 3 and 4 was studied by creating a null model for each subproteome under scrutiny. This approach enabled us to assess the statistical significance of a given result and consists of the comparison between a specific value and a distribution of values obtained from multiple random samples of the same size as the reference sample. Each delta-score Δ{s} associated with a subproteome {s} containing $n_s$ genes, obtained as a global average of the expression values of the group of genes of interest, was directly compared to a distribution of Δ scores, obtained by sampling the transcriptome of reference multiple times and by creating multiple random subproteomes of the same size $n_s$ as the reference subproteome. The P value was then the probability of obtaining a value more extreme than the empirical one, using the random distribution as a reference.

**Weighted gene co-expression network analysis.** Weighted gene co-expression network analysis is a data mining method that allows the quantification and interpretation of correlations between variables. In biology, this approach is widely used to study the covariation of genes and proteins across different samples and conditions (different cell types in our analysis). It is based on the definition of a similarity measure, the Pearson's correlation coefficient in our case, which serves as a parameter to build the topology of the network. The Pearson's correlation coefficient is defined as

$$\rho_{X,Y} = \frac{cov(X,Y)}{\sigma_X \sigma_Y}$$

where $cov(X, Y) = [(X - \mu_X)(Y - \mu_Y)]$ is the covariance among genes $X$ and $Y$ across the cell types (with $\mu_X$ and $\mu_Y$ being the mean values of $X$ and $Y$, respectively), and $\sigma_X$ and $\sigma_Y$ are their s.d. values. Different measures are possible to quantify the centrality of each gene in the network. We selected the total degree of a node, defined as the weighted sum of the links connecting it to all the other nodes in the network, with each link being weighted by the Pearson's correlation coefficient computed above.

**Single-molecule fluorescent in situ hybridization (sm-FISH).** Fresh-frozen sections from healthy adults were fixed while frozen in 4% PFA and stained with human-specific RNA probes (*MAPT/MAPK1/FKBP5*-C1, *SLC17A7*-C2 and *GAD1*-C3; *SLC17A7*-C1, *ENC1*-C2, and *GAD1*-C3) using the RNAscope Multiplex Fluorescence Kit according to the manufacturer's instructions. After staining, background lipofuscin autofluorescence was quenched using 1% True black (Biotium). Following nucleus counterstaining with DAPI, sections were mounted with ProLong gold antifade reagent. Stained sections were imaged by confocal laser scanning microscopy (LSM800, Zeiss) with a 63× objective. Images were taken across the superficial layers of the EC or BA9 to ensure reproducibility, totaling 10 images per section. Single-mRNA signals from 40 EX and 40 IN neurons (10 neurons from each human brain, 4 brains in total) were manually quantified using the ZEN 2 (blue edition, Zeiss), and the results were expressed as the percentage of the average count of single-mRNAs in IN neurons. Data was analyzed and graphed using Prism 5 software (GraphPad).

**Mouse primary cortical neuron culture and viral transduction.** Primary mouse neurons were prepared from embryonic day 16–18 mouse embryos and cultured as described with some modifications[41]. All procedures were approved and performed in compliance with the University of Rochester guidelines for the care and use of laboratory animals. In brief, cerebral cortices were isolated from the mouse brains, meninges were removed, and then the cortices were transferred into Trypsin-EDTA (0.05%) and digested for 15 min. Following gentle trituration, neurons were plated at a density of 15,000 cells/cm$^2$ on poly-D-lysine-coated (Sigma) coverslips for imaging. Neurons were grown for 24–26 days in vitro (DIV) in maintenance media (Neurobasal-A medium supplemented with 2% B27 and 2 mM GlutaMax), and half of media was replaced every 3–4 d. For lentiviral transduction, DIV14 neurons were treated with scrambled or shBAG3 without GFP virus in a half-volume of growth media for 16 h, and then the conditioned media, supplemented with an equal volume of fresh media, was added back.

**Immunofluorescence staining of endogenous tau accumulation in primary neurons.** Eleven days after transduction with scrambled or shBAG3 virus, the neurons were rinsed with PBS twice, then fixed in PBS containing 4% paraformaldehyde and 4% sucrose for 5 min at room temperature. Cells were then permeabilized in PBS containing 0.25% Triton X-100 for 10 min at room temperature and were blocked with PBS containing 5% BSA and 0.3 M glycine. Primary antibodies were diluted in blocking solution as follows: goat anti-GAD, 1:1,000; rabbit anti-TBR1, 1:500; mouse anti-12E8, 1:2,000; neurons were incubated with antibodies on a shaker at 4 °C overnight. The next day, neurons were washed with PBS three times for 10 min each time. Alexa Fluor 488-conjugated donkey anti-rabbit IgG (1:1,000), Alexa Fluor 594-conjugated donkey anti-mouse IgG (1:1,000), or Alexa Fluor 647-conjugated donkey anti-goat IgG (1:1,000) was diluted in blocking solution and incubated with neurons for 1 h at room temperature. After 3 × 10 min washes, neurons were incubated with Hoechst 33342 (2 μM) for 10 min at room temperature, then coverslips were mounted with ProLong diamond antifade mountant. Images were acquired on the laser scanning confocal microscope (LSM800, Zeiss) via z-stack. The maximum z projection of those images was used for looking at the tau puncta in the neurites.

**Western blot analysis.** Primary cortical neurons cultured in six-well plates were transduced with scramble, shBAG3, or BAG3 OE lentivirus for 7 d, and the total protein lysates were prepared and subjected to western blot assay as previously described[42]. We electrophoretically separated 2.5 μg of protein lysates on 4–12% Bis-Tris precast polyacrylamide gels and blotted them onto nitrocellulose blotting membranes. Blots were probed with rabbit primary antibodies for BAG3 (1:5,000) or GAPDH (1:6,000). After washing and incubation with secondary horseradish peroxidase-conjugated antibodies, membranes were developed with ECL, and digitalized images were taken using a Fujifilm LAS-3000 Imager.

**Neuronal culture, viral transduction, and tau seeding experiment.** Primary neuronal cultures were prepared and maintained as previously described[43]. At DIV2, neurons cultured on poly-D-lysine-coated coverslips were transduced with the scrambled BAG3, shBAG3, or BAG3 OE lentivirus. Half of the media was changed and neurons were transduced with 2 μL of RD-P301S-YFP (1:100) lentivirus. At DIV5, the media was changed and cells were incubated with 7.5 μg of DS9 tau seeds (prepared in sterile PBS) overnight. The media was then changed into the growth media and incubated for an additional 4–6 d. The cells were fixed with 4% PFA at room temperature for 30 min and were subjected to immunofluorescent staining as described above. Cells were incubated with primary antibodies rabbit anti-TBR1 (1:750) and goat anti-GAD1 (1:750) at 4 °C overnight, followed by incubation with appropriate secondary donkey antibodies at room temperature for 2 h. Images were acquired on the laser scanning confocal microscope (LSM800, Zeiss) at 20× magnification, the whole view of which was used as the region of interest (ROI). Each group has four coverslips, and 20 images per coverslip at 1,024 × 1,024 resolution were taken randomly from all the orientations of the coverslip. The numbers of TBR1$^+$ EX and GAD1$^+$ IN neurons with tau inclusions were quantified blind to the treatment.

**Statistical analysis.** No statistical methods were used to predetermine sample sizes, but our sample sizes are similar to those reported in previous publications[38,39,43]. Prism 5 software was used to analyze the data. All data are expressed as mean ± s.e.m. We performed the D'Agostino–Pearson omnibus normality test to determine whether the data were normally distributed, or the $F$ test to determine whether the data assumed equal variances. We then chose the following statistical tests. Unpaired $t$ tests were used to compare numbers of neuronal marker-positive and MC1$^+$ cells in EC-tau and control mice. One-way ANOVA with Tukey's post hoc tests were used to compare the numbers of neuronal marker-positive cells in human brains at different Braak stages. Unpaired $t$ tests with Welch's corrections were used to compare numbers of MC1$^+$ cells in human brains, and the numbers of single-cell mRNAs between EX and IN neurons. Nonparametric Mann–Whitney tests were used to compare the mean intensity of BAG3 in human non-AD and AD. Nonparametric Kruskal–Wallis tests with Dunn's multiple-comparisons post hoc tests were used to compare co-localization ratios, the numbers of neurons with 12E8 tau$^+$ puncta, the numbers of TBR1$^+$ neurons with tau inclusions, and the numbers of GAD1$^+$ neurons with tau inclusions. All results represent two-sided tests comparing groups of biological replicates. $P < 0.05$ was considered statistically significant for all measures. The $n$ values represent the number of animals, neurons, or brains in each group; exact values are indicated in figure legends.

**Reporting Summary.** Further information on research design is available in the Nature Research Reporting Summary linked to this article.

## Data availability
The data used to generate the results that support the findings of this study are available from the corresponding authors upon reasonable request.

## References

37. Seubert, P. et al. Detection of phosphorylated Ser262 in fetal tau, adult tau, and paired helical filament tau. *J. Biol. Chem.* **270**, 18917–18922 (1995).
38. Sanders, D. W. et al. Distinct tau prion strains propagate in cells and mice and define different tauopathies. *Neuron* **82**, 1271–1288 (2014).
39. Fu, H. et al. Tau pathology induces excitatory neuron loss, grid cell dysfunction, and spatial memory deficits reminiscent of early Alzheimer's disease. *Neuron* **93**, 533–541.e5 (2017).
40. Tasic, B. et al. Adult mouse cortical cell taxonomy revealed by single cell transcriptomics. *Nat. Neurosci.* **19**, 335–346 (2016).
41. Ji, C., Steimle, B. L., Bailey, D. K. & Kosman, D. J. The ferroxidase hephaestin but not amyloid precursor protein is required for ferroportin-supported iron efflux in primary hippocampal neurons. *Cell. Mol. Neurobiol.* **38**, 941–954 (2018).
42. Tosto, G. et al. F-box/LRR-repeat protein 7 is genetically associated with Alzheimer's disease. *Ann. Clin. Transl. Neurol* **2**, 810–820 (2015).
43. Wu, J. W. et al. Small misfolded Tau species are internalized via bulk endocytosis and anterogradely and retrogradely transported in neurons. *J. Biol. Chem.* **288**, 1856–1870 (2013).

Corresponding author(s): Karen Duff, Hongjun Fu, Michele Vendruscolo

# Reporting Summary

Nature Research wishes to improve the reproducibility of the work that we publish. This form provides structure for consistency and transparency in reporting. For further information on Nature Research policies, see Authors & Referees and the Editorial Policy Checklist.

## Statistical parameters

When statistical analyses are reported, confirm that the following items are present in the relevant location (e.g. figure legend, table legend, main text, or Methods section).

| n/a | Confirmed | |
|---|---|---|
| ☐ | ☒ | The exact sample size ($n$) for each experimental group/condition, given as a discrete number and unit of measurement |
| ☐ | ☒ | An indication of whether measurements were taken from distinct samples or whether the same sample was measured repeatedly |
| ☐ | ☒ | The statistical test(s) used AND whether they are one- or two-sided
*Only common tests should be described solely by name; describe more complex techniques in the Methods section.* |
| ☐ | ☒ | A description of all covariates tested |
| ☐ | ☒ | A description of any assumptions or corrections, such as tests of normality and adjustment for multiple comparisons |
| ☐ | ☒ | A full description of the statistics including central tendency (e.g. means) or other basic estimates (e.g. regression coefficient) AND variation (e.g. standard deviation) or associated estimates of uncertainty (e.g. confidence intervals) |
| ☐ | ☒ | For null hypothesis testing, the test statistic (e.g. $F$, $t$, $r$) with confidence intervals, effect sizes, degrees of freedom and $P$ value noted
*Give P values as exact values whenever suitable.* |
| ☒ | ☐ | For Bayesian analysis, information on the choice of priors and Markov chain Monte Carlo settings |
| ☒ | ☐ | For hierarchical and complex designs, identification of the appropriate level for tests and full reporting of outcomes |
| ☐ | ☒ | Estimates of effect sizes (e.g. Cohen's $d$, Pearson's $r$), indicating how they were calculated |
| ☐ | ☒ | Clearly defined error bars
*State explicitly what error bars represent (e.g. SD, SE, CI)* |

*Our web collection on statistics for biologists may be useful.*

## Software and code

Policy information about availability of computer code

| Data collection | No software was used. |
|---|---|
| Data analysis | Excel, ImageJ, ZEN 2 (blue edition), Python2.7 and Graphpad Prism 5.0 softwares were used. |

For manuscripts utilizing custom algorithms or software that are central to the research but not yet described in published literature, software must be made available to editors/reviewers upon request. We strongly encourage code deposition in a community repository (e.g. GitHub). See the Nature Research guidelines for submitting code & software for further information.

## Data

Policy information about availability of data

All manuscripts must include a data availability statement. This statement should provide the following information, where applicable:

- Accession codes, unique identifiers, or web links for publicly available datasets
- A list of figures that have associated raw data
- A description of any restrictions on data availability

All the datasets we used are publicly available datasets generated by other groups with accession codes indicated in the paper. All the raw data associated with all the figures and supplementary figures are available upon request. There is no restrictions on data availability.

# Field-specific reporting

Please select the best fit for your research. If you are not sure, read the appropriate sections before making your selection.

☒ Life sciences          ☐ Behavioural & social sciences          ☐ Ecological, evolutionary & environmental sciences

For a reference copy of the document with all sections, see nature.com/authors/policies/ReportingSummary-flat.pdf

# Life sciences study design

All studies must disclose on these points even when the disclosure is negative.

| | |
|---|---|
| Sample size | Sample size was reported in the 'Statistical analysis' section of the Methods and figure legends. The sample size for quantifying the number of neurons and single-mRNA molecules was based on previous publications for biological experiments as well as the property of our data, i.e. clear separation between excitatory neurons and inhibitory neurons. For single-nucleu RNA-seq datasets, there are 3227 single nuclei and 19,550 single nuclei in each dataset, which are enough based on previous single-nucleus RNA-seq analysis. |
| Data exclusions | In order to avoid biases in the analysis and reduce the amount of noise, the bottom 5% low quality samples (samples with less reads across the transcriptome) in DroNc-Seq dataset were discarded as they were considered to have been damaged during the experimental procedure. |
| Replication | In order to ensure our experimental findings can be reliably reproduced, we include appropriate number of animals, sections, and neurons as listed in the figure legends. Further, three independent experiments were repeated with similar results. Also, the staining has been repeated by three persons in the lab independently. <br> In order to ensure our experimental findings can be reliably reproduced, we include appropriate number of animals, sections, and neurons as listed in the figure legends. Further, three independent experiments were repeated with similar results. Also, the staining has been repeated by three persons in the lab independently. |
| Randomization | The experimental groups were allocated by the animal genotype, human case information, and the treatment. The covariants of age, gender, culture days, and vehicle were controlled as the same between experimental groups. Further, the sections, coverslips and neurons within each group were selected randomly. 10 images per sm-FISH stained section was randomly taken from the superficial layers of the entorhinal cortex or BA9 region. 60 excitatory and 60 inhibitory neurons from 3 human non-AD and AD sections were randomly selected for comparing the mean intensity of BAG3. Also, 5 excitatory and 5 inhibitory neurons from each coverslip (n = 11 coverslips each group) were randomly taken for comparing the endogenous 12E8 tau+ punta in neurites. Additionally, 20 images per coverslip at 1,024 × 1,024 resolution were taken randomly from all the orientations of the coverslip for the tau seeding experiment. The number of TBR1+ EX and GAD1+ IN neurons with tau inclusions were quantified blindly. |
| Blinding | The experimenter was blind to the experimental groups when they performed the immunostaining and sm-FISH as well as the counting of neurons and the single-mRNA molecules, and the comparison of the mean intensity of BAG3. |

# Reporting for specific materials, systems and methods

## Materials & experimental systems

| n/a | Involved in the study |
|---|---|
| ☐ | ☒ Unique biological materials |
| ☐ | ☒ Antibodies |
| ☒ | ☐ Eukaryotic cell lines |
| ☒ | ☐ Palaeontology |
| ☐ | ☒ Animals and other organisms |
| ☒ | ☐ Human research participants |

## Methods

| n/a | Involved in the study |
|---|---|
| ☒ | ☐ ChIP-seq |
| ☒ | ☐ Flow cytometry |
| ☒ | ☐ MRI-based neuroimaging |

## Unique biological materials

Policy information about availability of materials

| | |
|---|---|
| Obtaining unique materials | The Tau RD-P301S-YFP lentivirus and DS9 clone cell lines were provided by Dr. Marc Diamond. The BAG3 shRNA and the shRNA-resistant BAG3 were provided by Dr. Gail Johnson. All the brain tissue were provided by New York Brain Bank and Banner Sun Health Research Institute Brain and Body Donation Program. |

# Antibodies

| | |
|---|---|
| Antibodies used | Human conformation-dependent tau (MC1, 1:750) and human/murine phospho-tau pSer396/ Ser404 (PHF1, 1:500) monoclonal antibodies were provided by Dr. Peter Davies. Mouse anti-phosphorylated tau Ser262 and/or Ser356 (12E8, 1:2000) antibody is a kind gift from Dr. Philip Dolan. Human/murine phospho-tau pSer202/Thr205 (AT8, Cat# MN1020, 1:500) and pThr212/Ser214 (AT100, Cat# MN1060, 1:500) monoclonal antibodies, rabbit anti-phospho-tau pSer422 (pS422, Cat# 44-764G, 1:250) and parvalbumin (PVALB, Cat# PA5-18389, 1:1000) polyclonal antibodies, Alexa Fluor dye-labeled cross-absorbed goat and donkey secondary antibodies (Cat# A-11029, A-11037, A-11007, A-11058, and A-21202, 1:1000) were purchased from Thermo Fisher Scientific. Rabbit anti-TBR1 (Cat# ab31940, 1:250) and SATB2 (Cat# ab92446, 1:250) polyclonal antibodies were purchased from Abcam. Rat anti-somatostatin (SST) (Cat# MAB354, 1:100) and mouse anti-NeuN (Cat# MAB377, 1:250) monoclonal antibody and goat anti-GAD1 (Cat# AF2086, 1:100) polyclonal antibody were purchased from Millipore and R&D Systems, respectively. Rabbit anti-calretinin (CALB2) (Cat# 7697, 1:1000), IBA-1 (Cat# 019-19741, 1:500), and GFAP (Cat# G9269, 1:2500) polyclonal antibodies were purchased from Swant, Wako and Sigma-Aldrich, respectively. Rabbit anti-TBR1 (Cat# 20932-1-AP, 1:250) and rabbit anti-BAG3 (Cat# 10599-1-AP, 1:100) polyclonal antibody were purchased from Proteintech Group. |
| Validation | All of them have been used in previous publications and validated by the manufacturers or research scientists. <br> MC1: validated in Neurobiol Aging. 2000 Sep-Oct;21(5):719-27; https://www.alzforum.org/antibodies/tau-mc1 <br> PHF1: validated in https://www.alzforum.org/antibodies/tau-phos-ser396ser404-phf-1 <br> 12E8: validated in https://www.alzforum.org/antibodies/tau-12e8 <br> AT8: validated in https://www.thermofisher.com/antibody/product/Phospho-Tau-Ser202-Thr205-Antibody-clone-AT8-Monoclonal/MN1020 <br> AT100: validated in https://www.thermofisher.com/antibody/product/Phospho-Tau-Thr212-Ser214-Antibody-clone-AT100-Monoclonal/MN1060 <br> pS422: validated in https://www.thermofisher.com/antibody/product/Phospho-Tau-Ser422-Antibody-Polyclonal/44-764G <br> PVALB: validated in https://www.thermofisher.com/antibody/product/Parvalbumin-Antibody-Polyclonal/PA5-18389 <br> TBR1: validated in http://www.ptglab.com/Products/TBR1-Antibody-20932-1-AP.htm#validation <br> SATB2: validated in https://www.abcam.com/satb2-antibody-epncir130a-ab92446.html <br> SST: validated in http://www.emdmillipore.com/US/en/product/Anti-Somatostatin-Antibody-clone-YC7,MM_NF-MAB354#overview <br> NeuN: validated in http://www.emdmillipore.com/US/en/product/Anti-NeuN-Antibody-clone-A60,MM_NF-MAB377 <br> GAD1: validated in https://www.rndsystems.com/products/human-mouse-rat-gad1-gad67-antibody_af2086 <br> calretinin : validated in https://www.swant.com/?p=products&c=1.2 <br> IBA-1: validated in http://www.wako-chem.co.jp/english/labchem/product/life/AntiIba1/index.htm <br> GFAP: validated in https://www.sigmaaldrich.com/catalog/product/sigma/g9269?lang=en&region=US <br> BAG3: validated in https://www.ptglab.com/products/BAG3-Antibody-10599-1-AP.htm#validation |

# Animals and other organisms

Policy information about studies involving animals; ARRIVE guidelines recommended for reporting animal research

| | |
|---|---|
| Laboratory animals | The species, strain, sex and age of the laboratory animals used in this study have been clearly written in the paper. The F1 mouse offspring (both males and females at 22 and 30+ months old, strain FVB/N:C57BL/6) were used as experimental animals. All animals were maintained on a 12 hr light/dark cycle with food and water provided ad libitum. All animal experiments were performed in accordance with national guidelines (National Institutes of Health) and approved by the Institutional Animal Care and Use Committee of Columbia University. Primary cortical neuron culture were prepared from and embryonic day 16-18 embryos from C57BL/6 mice. |
| Wild animals | This study does not include wild animals. |
| Field-collected samples | This study does not include the samples collected from the field. |